Effects of sediment properties, distance from source, and frequency weighting on sound pressure and sound pressure kurtosis for marine airgun signaturesa)

Sertlek, H. Özkan; Peng, Yaxi; Ainslie, Michael A.; von Benda-Beckmann, Alexander M.; Halvorsen, Michele B.; Koessler, Matthew W.; Küsel, Elizabeth T.; MacGillivray, Alexander O.; Tsouvalas, Apostolos

DOI
10.1121/10.0034709

Publication date
2024

Document Version
Final published version

Published in
Journal of the Acoustical Society of America

DECEMBER 24 2024

Effects of sediment properties, distance from source, and frequency weighting on sound pressure and sound pressure kurtosis for marine airgun signatures[a)]

H. Özkan Sertlek ; Yaxi Peng; Michael A. Ainslie ; Alexander M. von Benda-Beckmann ;
Michele B. Halvorsen ; Matthew W. Koessler; Elizabeth T. Küsel; Alexander O. MacGillivray ;
Apostolos Tsouvalas

J. Acoust. Soc. Am. 156, 4242–4255 (2024)
https://doi.org/10.1121/10.0034709

JASA ARTICLE

Effects of sediment properties, distance from source, and frequency weighting on sound pressure and sound pressure kurtosis for marine airgun signatures[a)]

H. Özkan Sertlek,[1,2,b)] Yaxi Peng,[2] Michael A. Ainslie,[1] Alexander M. von Benda-Beckmann,[3] Michele B. Halvorsen,[4] Matthew W. Koessler,[5] Elizabeth T. Küsel,[4] Alexander O. MacGillivray,[5] and Apostolos Tsouvalas[2]

[1]*JASCO Applied Sciences (Deutschland) GmbH, Schwentinental, Germany*

[2]*Faculty of Civil Engineering and Geosciences, Delft University of Technology, Stevinweg 1, 2628 CN, Delft, The Netherlands*

[3]*TNO, Acoustic Sensor and Sonar Systems, The Hague, The Netherlands*

[4]*JASCO Applied Sciences (USA), Inc., Silver Spring, Maryland 20910, USA*

[5]*JASCO Applied Sciences (Canada), Ltd., Victoria, Canada*

ABSTRACT:

Investigation of sound pressure waveforms helps the selection of appropriate metrics to evaluate their effects on marine life in relation to noise thresholds. As marine animals move farther away from a sound source, the temporal characteristics of sound pressure may be influenced by interactions with the sediment and the sea surface. Sound pressure kurtosis and root-mean-square (rms) sound pressure are quantitative characteristics that depend on the shape of a sound pulse, with kurtosis related to the qualitative characteristic "impulsiveness." After verifying the propagation modeling approach using selected test cases from the JAM Workshop held in Cambridge, UK, in 2022, the time dispersion values of pressure signals produced by an individual airgun shot across various sediment types are analyzed. The results reveal that there is significant pulse dispersion when the seabed consists of predominantly sand-type sediments: i.e., the airgun signal duration increases considerably over long distances, thus decreasing the kurtosis of a sequence of pulses, whereas the pulse dispersion is more limited for clay and silt-type sediments. The range variations of frequency weighted kurtosis and rms sound pressure differ from those of the unweighted kurtosis, depending on the corresponding lower and upper roll-off frequencies corresponding to different marine animal groups. https://doi.org/10.1121/10.0034709

(Received 29 February 2024; revised 28 November 2024; accepted 3 December 2024; published online 24 December 2024)

[Editor: James F. Lynch] Pages: 4242–4255

I. INTRODUCTION

The underwater sound produced by anthropogenic activities can lead to various impacts on aquatic life, including physical injuries, shifts in hearing thresholds (both permanent and temporary), and alterations in the behavior of marine species (Carroll *et al.*, 2017; Erbe *et al.*, 2022). To assess the potential impact comprehensively, researchers have defined various impact thresholds for marine mammals (Southall *et al.*, 2019). These thresholds provide crucial benchmarks for assessing the effects of anthropogenic activities on marine ecosystems. Proposed thresholds account for differences between "pulse" and "non-pulse" sounds, where it is found that the animal hearing organ is more susceptible to auditory injury from impulsive sounds. Furthermore, appropriate auditory weighting functions could be used to account for differences in frequency-selective hearing sensitivity of different marine animal groups. The bandwidth of sound signals, time-dependence, as well as auditory hearing functions are thus critical as they play an important role in impact assessment studies. The variations in bandwidth for the analysis can affect the kurtosis and root-mean-square (rms) sound pressure, depending on how the sound energy is distributed across frequencies for different source signals.

Due to the high levels and impulsive nature of sound generated by marine airgun operations, this is one of several sound sources that are of particular concern when it comes to impact on marine life (Slabbekoorn *et al.*, 2010; Gedamke *et al.*, 2011; Slabbekoorn *et al.*, 2019; Merchant *et al.*, 2020; Prior *et al.*, 2021; Sidorovskaia and Li, 2022). When marine airgun operations take place in shallow waters, sound waves reflect multiple times from the sea surface and the seabed. Airgun pulses cover a wide frequency band; they are characterised by several frequency components, each traveling at its own group velocity, leading to different arrival times at the receiver location. Consequently, the time signal at a receiver's location is dispersed, i.e., is altered in both duration and amplitude,

[a)]This paper is part of a special issue on Verification and Validation of Source and Propagation Models for Underwater Sound.

[b)]Email: osertlek@gmail.com

compared to the signal at the source (Sertlek and Aksoy 2013; Guan *et al.*, 2015). This dispersion of the time signal makes the categorisation of the sound sources ambiguous and the choice of the impact criteria challenging (Hastie *et al.*, 2019; Martin *et al.*, 2020).

Quantitative approaches are being explored to apply a single impact threshold to describe the impulsiveness of underwater sounds that can account for the characteristics of the signals based on kurtosis of the pressure waveform (von Benda-Beckmann *et al.*, 2022; Zeddies *et al.*, 2023). Kurtosis, a statistical measure (Müller *et al.*, 2020), has been proposed as a quantitative alternative to the "impulsiveness" of time domain underwater acoustic signals (Martin *et al.*, 2020). The use of kurtosis has primarily been driven by hearing studies in humans and land mammals that indicate that growth of hearing loss is better predicted when including kurtosis of the signal than when just using the conventional equal-energy rule (Zhao *et al.*, 2010; Goley *et al.*, 2011; Henderson and Hamernik, 2012; Kastelein *et al.*, 2017). In previous studies, kurtosis has been determined for various underwater noise sources, such as airguns, pile-driving, underwater explosions, and sonar for a limited number of conditions, and has shown to vary depending on the source type. In practice, through propagation effects the kurtosis of a signal will also change with distance.

To provide insight into how the shape of the airgun pulse is affected by its environment through sound propagation and auditory filtering, this paper investigates the effect of the sediment types and range on the time dispersion of sound pressure signals created by a single airgun shot in shallow waters. The focus is placed on the determination of kurtosis of the signal and rms sound pressure under different environmental conditions. Simulations are based on a shallow water test case from JIP Acoustic Modelling (JAM) Workshop, held in Cambridge, UK, in 2022 (Ainslie *et al.*, 2024). First, the proposed modelling approach to calculate sound pressure is verified by multi-model comparisons, including normal modes, parabolic equation, and wave number integration methods. Following the model verification study, the time dispersion of the sound pressure at different distances is investigated for both the workshop test case and its modified version by replacing the half-space sediment layer with other possible sediment types. The sound pressure is weighted based on the selected auditory weighting functions for marine mammals (Southall *et al.*, 2019) and fishes (Lucke *et al.*, 2024). The sound pressure kurtosis and rms sound pressure, based on both unweighted and weighted sound pressures, are calculated for different sediment types at selected ranges. In all discussion hereafter, the underwater acoustical terminology follows ISO 18405:2017 (ISO, 2017).

II. SOUND PROPAGATION, KURTOSIS, AND RMS SOUND PRESSURE

A. Airgun source signature

Marine airguns find widespread use in exploring oil and gas reserves beneath the ocean's sediment layers. During an airgun shot, compressed air in the airgun chamber is rapidly released, creating a bubble in the water (Dragoset, 1990; Laws *et al.*, 1990; Caldwell and Dragoset, 2000). Because airguns are typically positioned close to the sea surface, around 5–6 m deep, their signals strongly interact with the sea surface. The upward-traveling sound wave reflects off the sea surface, giving rise to a down-going wave with a time delay, commonly referred to as the "surface ghost" and affected by the sea surface reflectivity at different sea states (Sertlek and Blacquière, 2019). Airguns are typically clustered in arrays to direct the acoustic beam towards the seabed with increased amplitude.

Airgun source signatures can be estimated on the basis of mathematical solutions of a system of coupled differential equations, including various physics-based models such as air-bubble hydrodynamics, gas pressure, thermodynamics, and mass transfer laws (Ziolkowski, 1970; Laws *et al.*, 1990; MacGillivray, 2006). The accuracies of different airgun modelling approaches were compared in different workshops, including various scenarios with single airgun shots and several airguns positioned in an array. Marine airgun modelling workshops were held in Dublin, Ireland, in 2016 (Ainslie *et al.*, 2019; Halvorsen *et al.*, 2019) and Cambridge, UK, in 2022 (Ainslie *et al.*, 2024). To investigate the developments of the modelling approaches, the same test case was included in both workshops for calculating the time dispersion from a single airgun shot at specified distances. The notional source signature of a single airgun scenario (described as the "S1" test case in the first Airgun Modelling Workshop 2016 in Dublin), which is calculated using an open-source airgun modelling software (AGORA) (Sertlek and Ainslie, 2015), was also used for Scenario B1 of the second airgun modelling workshop (JAM Workshop) in Cambridge. The time domain source waveform and frequency spectrum of the single airgun source signature are shown in Fig. 1.

Based on this airgun source waveform, the sound pressure in the time domain, which is required to calculate the kurtosis and rms sound pressure, is calculated at the horizontal distances 30 m, 300 m, and 3 km. In Sec. II C, the detailed description of the propagation model and its comparisons with other propagation models are described.

B. Calculation of kurtosis and rms sound pressure

The kurtosis and rms sound pressure are the quantities that can be directly calculated from the pressure in the time domain. Kurtosis is a statistical measure that quantifies the length of tails in the input data. It is not influenced by the scaling of the amplitude of signals. Müller *et al.* (2020) applied kurtosis to the time domain sound pressure signals and summarized its detailed properties. The sound pressure kurtosis, β, is calculated as

$$\beta = \frac{\mu_4}{\mu_2^2}, \quad (1)$$

where

https://doi.org/10.1121/10.0034709

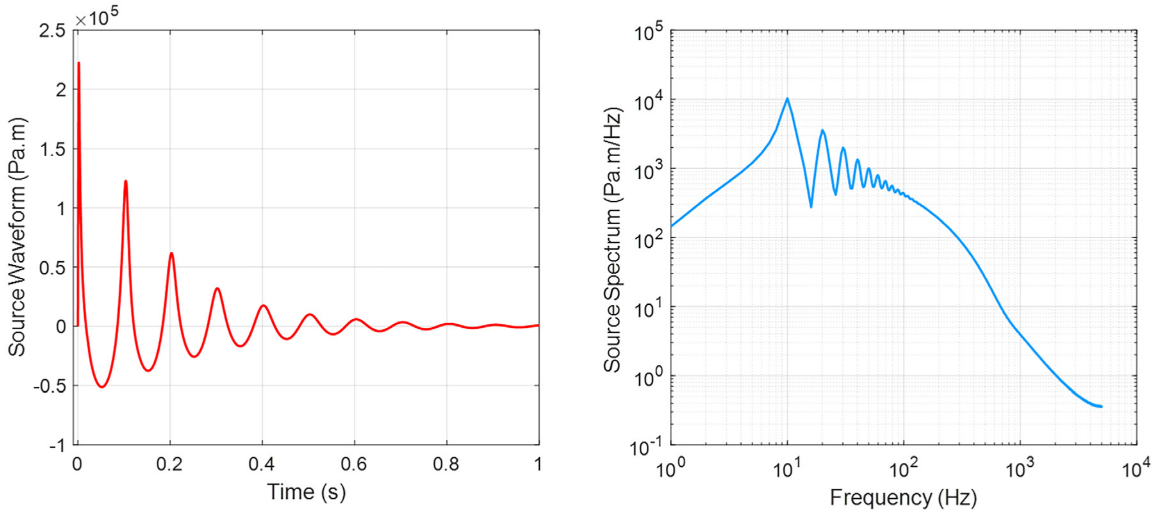

FIG. 1. (Color online) Airgun source waveform (left) and spectrum (right).

$$\mu_4 = \frac{1}{t_1 - t_0}\int_{t_0}^{t_1} [p(t) - \overline{p}]^4 dt,$$

$$\mu_2 = \frac{1}{t_1 - t_0}\int_{t_0}^{t_1} [p(t) - \overline{p}]^2 dt$$

is the sound pressure variance, $p(t)$ is sound pressure, $\overline{p}$ is mean sound pressure, and t_0 and t_1 are the time points where the signal starts and ends, respectively [ISO 18405:2017 (ISO, 2017)].

The rms sound pressure is calculated as

$$p_{\mathrm{rms}} = \sqrt{\frac{1}{t_1 - t_0}\int_{t_0}^{t_1} p^2(t)dt}. \tag{2}$$

It is related to the mean square sound pressure, as described in ISO 18405:2017 (ISO, 2017). A temporal observation window with 0.1 s duration is applied as a sliding time window to calculate rms sound pressure, representative of marine mammal auditory integration time (Lucke *et al.*, 2024).

C. Propagation modelling and verification tests

The sound pressure can be modeled in the time domain to be used in the kurtosis and rms sound pressure calculations. For this purpose, it is critical to choose an appropriate propagation modelling approach that can provide accurate results over a wide frequency band based on the source spectrum of the airgun used in this study. For the calculation of the time dispersion at the different range points, the SILENCE model, which is based on the complex wave number integration method, is used (Peng *et al.*, 2021). SILENCE was originally developed for modeling pile-driving sound, including the effect of a layered elastic sediment. It is capable of generating pressure, velocity, displacement, and stress fields. The original version of the model is coupled with a pile-driving source model (Tsouvalas and Metrikine, 2014). However, in this study, it has been modified slightly to calculate propagation loss for a point source in a Pekeris waveguide without elastic sediment properties to solve the test cases from the JAM Workshop (Ainslie *et al.*, 2024). The pressure field of Pekeris ocean environment is represented as a finite sum of modes and a complex wavenumber integral with the use of the Ewing–Jardetzky–Press (EJP) cut (Buckingham and Giddens, 2006). The solution is extended from two fluid layers into the case of a fluid layer overlying a solid bottom half-space, as discussed in Peng *et al.* (2021). The detailed mathematical description of the propagation model is given in the Appendix. The accuracy of the SILENCE model is verified by comparing the propagation loss (PL) outputs with other well-known propagation model results. The propagation models used in the multi-model comparisons are listed in Table I.

In these comparisons, the shallow water test case (A1) from the JAM Workshop in 2022 is used (Ainslie *et al.*, 2024). The test case scenario, A1, is based on a Pekeris waveguide with a water depth of 50 m for a sand-type seabed. A constant sound speed of 1500 m/s is used. The source and receiver depths are 5 m and 15 m, respectively. The problem geometry is shown in Fig. 2.

The comparisons are performed for ranges up to 30 km at 50, 100, 500, and 1000 Hz, as shown in Fig. 3.

TABLE I. Propagation models in the model verifications.

Model type	Model
Normal mode models	KRAKENC (Porter, 1992)
Wavenumber integration models	OASES (Schmidt, 2004)
	SCOOTER (Porter, 1992)
	SILENCE (Peng *et al.*, 2021)
Parabolic equation models	RAM (Collins, 1993)
	FWRAM (MacGillivray and Chapman, 2012)

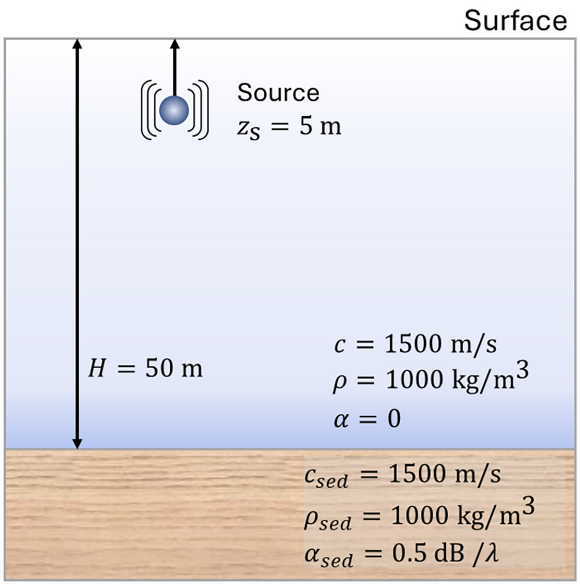

FIG. 2. (Color online) Problem geometry. Adapted from Fig. 1 of Ainslie et al. (2024).

The propagation loss results from SILENCE model agree with the other well-known propagation modelling results. A comprehensive analysis of the specific variances among these propagation models is beyond the scope of this paper. Such a comparison has already been extensively covered in previous publications (Küsel and Siderius, 2019; Sertlek *et al.*, 2019).

The time dispersion resulting from a single airgun shot can be determined at various distances using Fourier analysis. Initially, a frequency domain transfer function is computed by running the propagation model for each frequency component included in the source spectrum. Subsequently, this transfer function is multiplied by the airgun source spectrum. Finally, the time dispersion is calculated through an inverse Fourier transformation of this product. As an example, a verification test case, B1, from the JAM Workshop is used (Ainslie *et al.*, 2024). Based on this test case, the time dispersion from the single airgun shot shown in Fig. 1 is calculated at 300 and 3000 m. The transfer function is calculated between 2.75 Hz and 2818.5 Hz, as defined in the workshop scenarios. The frequency resolution in the calculation is chosen as 0.25 Hz. SILENCE's results are verified by comparing with FWRAM results at 30, 300, and 3000 m, as shown in Fig. 4. FWRAM is based on parabolic equation model that takes into full account the far-field, angle-dependent radiation pattern of the airgun array (MacGillivray and Chapman, 2012). More detailed comparisons between SILENCE and other propagation models (OASES, SCOOTER, and normal modes) are available from the JAM Workshop report (Ainslie *et al.*, 2023).

III. PARAMETRIC STUDY

The workshop test case is modified by replacing the sediment properties with some other potential sediment types. The properties of sediment types (representative grain size, sound speed, density and absorption) used in the comparisons are described in Table II (Ainslie, 2010). The sediment types are ranked by increasing order based on their representative grain sizes.

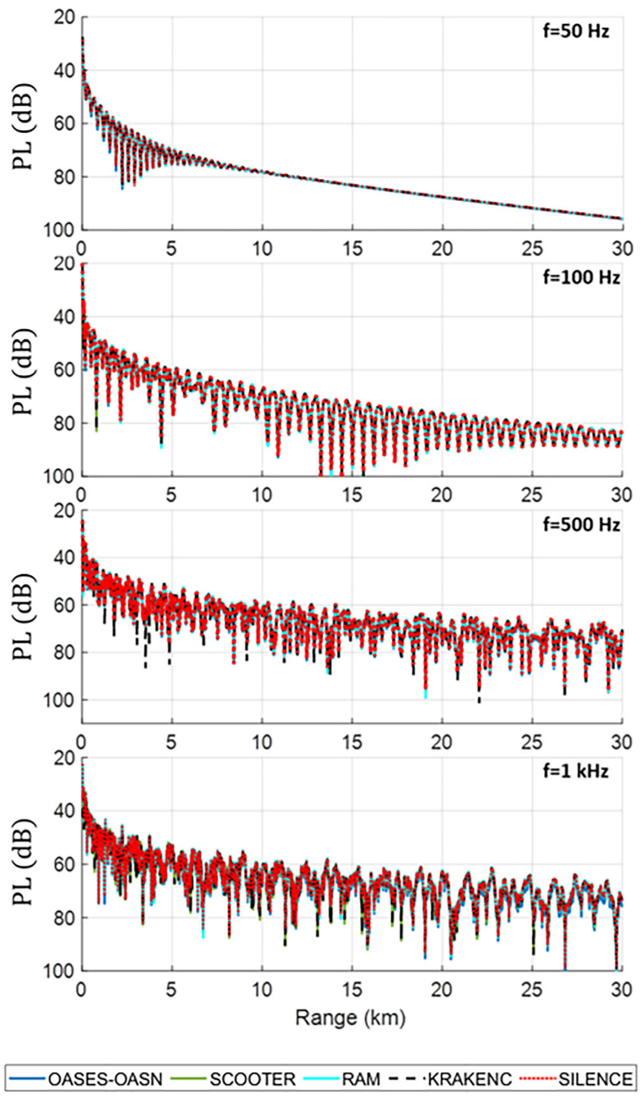

FIG. 3. (Color online) Comparison of propagation loss (PL) [re 1 m^2(dB)] results of SILENCE with other models at 50, 100, 500, and 1000 Hz.

A. Effect of bandwidth on sound pressure and kurtosis

Another factor that affects the time dispersion is the frequency bandwidth considered. In order to demonstrate the effect of bandwidth on the time dispersion, the calculations for the workshop case are repeated for the different frequency bands [based on the Svein Vaage dataset used during the JAM Workshop (Prior *et al.*, 2021; Ainslie *et al.*, 2024)], as listed in Table III. The time dispersion results are shown in Fig. 5.

When the lower frequency limit considered in the computation decreases, both the peak sound pressure and the kurtosis values are affected. When frequencies below 281.8 Hz are excluded from the computations (band 3), the

https://doi.org/10.1121/10.0034709

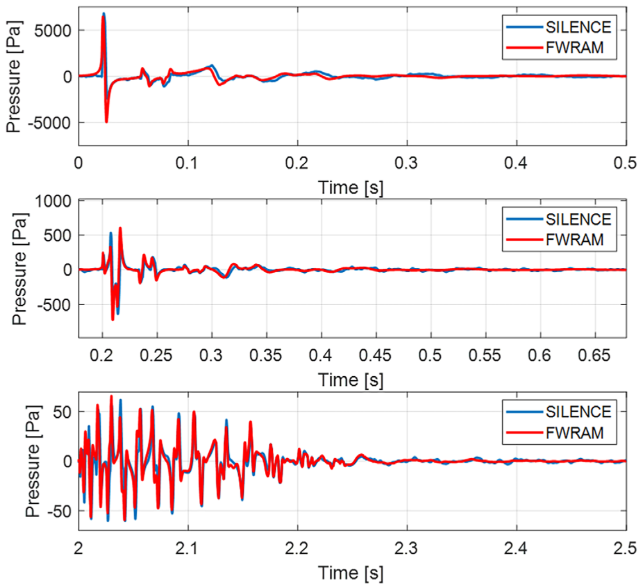

FIG. 4. (Color online) Comparison of the time domain waveforms calculated with different propagation models (SILENCE and FWRAM). Shown is sound pressure vs time for ranges 30 m (upper), 300 m (middle), and 3000 m (lower).

pressure values decrease considerably because most of the airgun energy is concentrated at these low frequencies outside the chosen bandwidth. Slight differences are visible between band 1 and band 2 results.

B. Time dispersion

The sound pressure at the selected receiver ranges as 30, 300, and 3000 m is plotted versus time in Fig. 6. The receiver depth is 15 m for these comparisons. Other parameters remain the same as in the workshop case except for the modifications in the sediment properties.

The time dispersion of airgun signals is significantly influenced by the properties of the sediment, and this influence is contingent on the number of reflections occurring between the sea surface and the sediment interface in the same ocean environment. When there are few interactions with the sediment at a distance of 30 m, the time domain sound pressure waveforms and sound exposure level (SEL) exhibit similarities across different sediment types. However, as the observation distance increases to 300 and 3000 m, the distinctive effect of sediment type becomes apparent. As time progresses beyond the initial wave front, discernible differences can be observed in the amplitude and duration of the pulse. The amplitude and duration of these waves increase with increasing soil impedance.

TABLE II. Properties of the sediment types used in the comparisons. The sound speed in water is 1500 m/s.

Sediment type	Representative grain size (ϕ)	Sound speed (m/s)	Density (kg/m^3)	Attenuation (dB/wavelength)
Coarse sand	0.5	1875	2231	0.87
Medium sand	1.5	1797	2086	0.88
Fine sand	2.5	1730	1945	0.89
Workshop case	—	1700	2000	0.5
Very fine sand	3.5	1670	1817	0.49
Coarse silt	4.5	1615	1702	1.22
Medium silt	5.5	1570	1601	0.38
Fine silt	6.5	1535	1513	0.17
Very fine silt	7.5	1510	1439	0.11
Coarse clay	8.5	1490	1378	0.08
Medium clay	9.5	1470	1331	0.09

TABLE III. Frequency bands used in the comparisons.

Frequency band	Minimum frequency (Hz)	Maximum frequency (Hz)
Band 1	2.818	2818
Band 2	28.18	2818
Band 3	281.8	2818

In the case of sand-type sediment, a greater portion of the sound energy remains in the water column, traveling through multiple reflections from both the sea surface and the seabed. In contrast, for silt- and clay-type sediments, a significant portion of the sound energy is transmitted into the sediment, resulting in lower signal amplitude and duration in the water and hence lower SEL values when compared to scenarios involving sand-type sediment.

C. Kurtosis and rms sound pressure

Based on the time domain pressure waveforms shown in Fig. 6, the kurtosis values can be calculated. The signal time duration is set to 10 s for the kurtosis calculations. Kurtosis calculations can simplify the analysis of the time-dispersion results and help to understand how pulse length is affected by sediment properties and range.

Kurtosis is independent of the amplitude of the sound pressure waveform. Thus, SEL, which is defined as $\mathrm{SEL} = 10\log_{10}(E_p/E_0)$ dB, where E_p is the sound exposure, is also calculated as complementary information, based on the same time domain pressure waveforms. For the SEL calculation, E_p is the time-integrated squared sound pressure and $E_0 = p_0^2 t_0 = 1\,\mu\mathrm{Pa}^2\,\mathrm{s}$ is the reference value of time-integrated squared sound pressure [ISO 18405:2017 (ISO, 2017)]. The reference sound pressure and time values are $p_0 = 1\,\mu\mathrm{Pa}$ and $t_0 = 1$ s, respectively.

For some sediment types (e.g., very fine silt and medium clay), sound pressure can decrease significantly over distance. In real-life scenarios, ambient sound is always present and can distort the time domain waveform. To illustrate this effect, Gaussian noise with a rms value of 1 Pa (corresponding to an SPL of 120 dB) is added to the time domain waveforms, as shown in Fig. 7. This addition helps obtain more realistic kurtosis values by disregarding low-amplitude sound pressures at long distances that fall below the ambient sound level.

In Fig. 8, the variations of kurtosis with and without adding Gaussian noise are shown for different sediment types and distances (as 30, 300, and 3000 m).

https://doi.org/10.1121/10.0034709

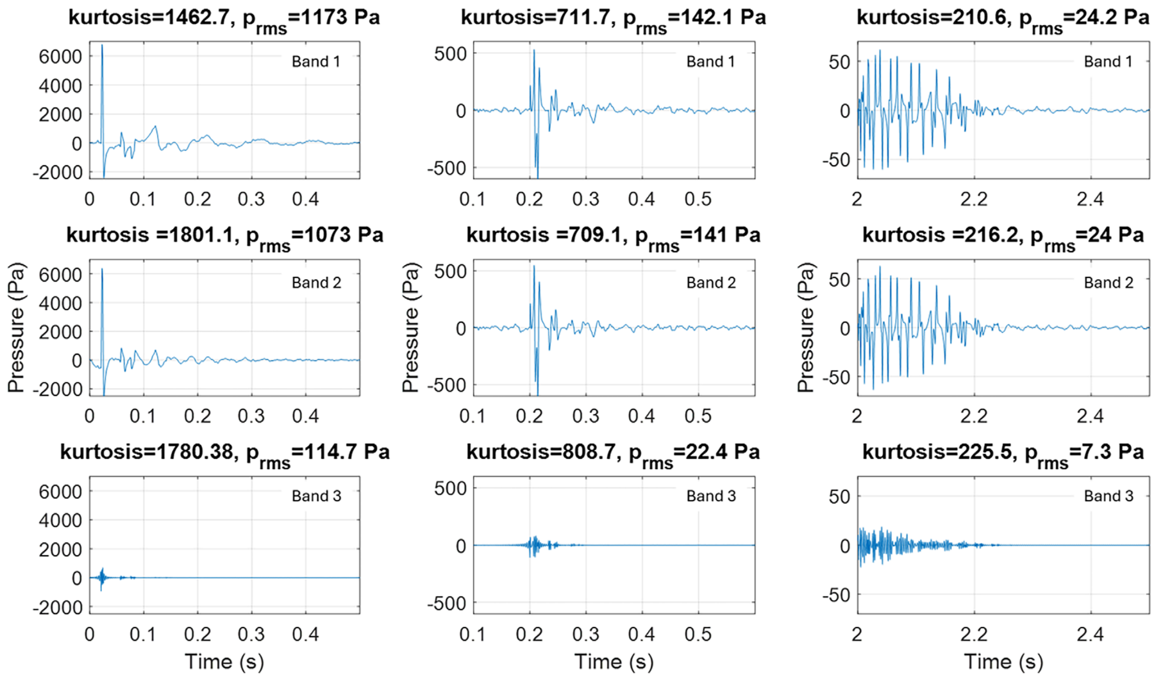

FIG. 5. (Color online) Time distribution calculations for different bandwidths. The sediment parameters from the workshop case are used. The minimum and maximum frequencies are listed in Table III.

Consistent with the findings in the preceding section, it is observed that sand-type sediments exhibit stronger reflections from the seabed in comparison to silt and clay sediments, leading to a notable impact on the kurtosis of the sound pressure (Fig. 9). After adding Gaussian noise, when the amplitude of sound pressure is very low (less than 6 Pa) at 3000 m, a lower kurtosis value, converging to the kurtosis of Gaussian noise (3), is observed, particularly for silt and clay sediments.

The range-dependent variation of the kurtosis, SEL, and peak sound pressure are shown for sand, silt, and clay sediment categories in Fig. 10.

As the range increases, the kurtosis decreases for scenarios involving sand-type sediments. Since most of the sound energy remains in the water layer, sand-type sediments exhibit the highest SEL values for the sand-type sediments. Conversely, for silt and clay sediment types, sound waves can easily penetrate the sediment layer, resulting in a

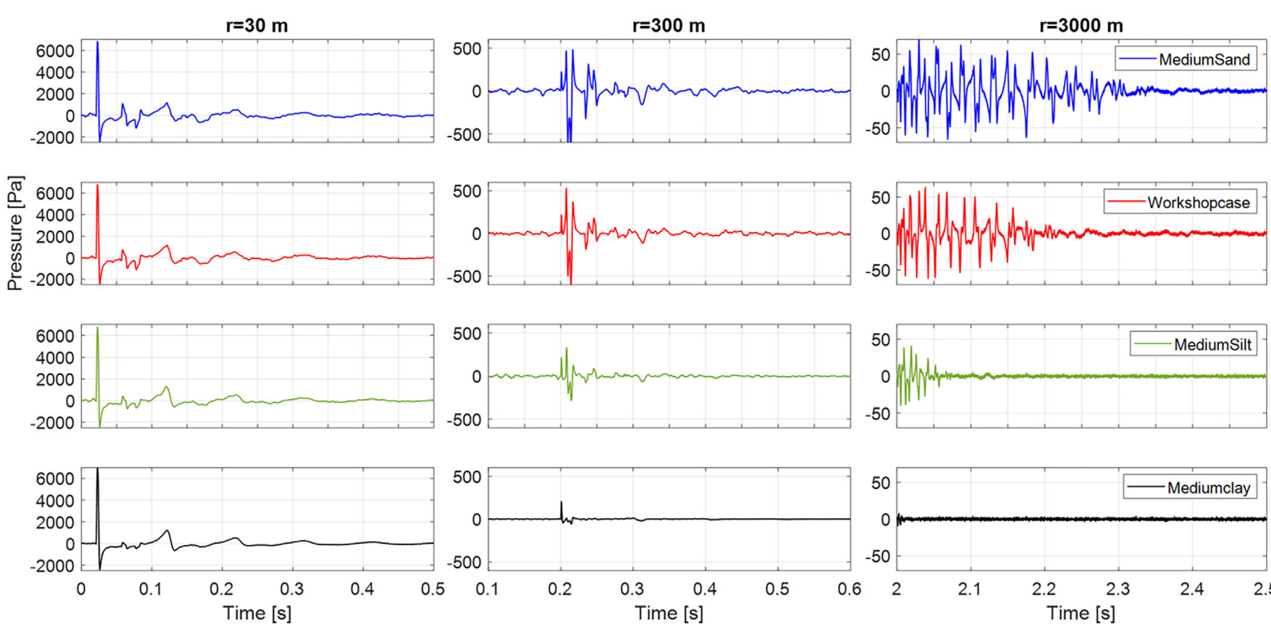

FIG. 6. (Color online) Sound pressures at 30 m (left), 300 m (middle), and 3000 m (right) for different sediment types.

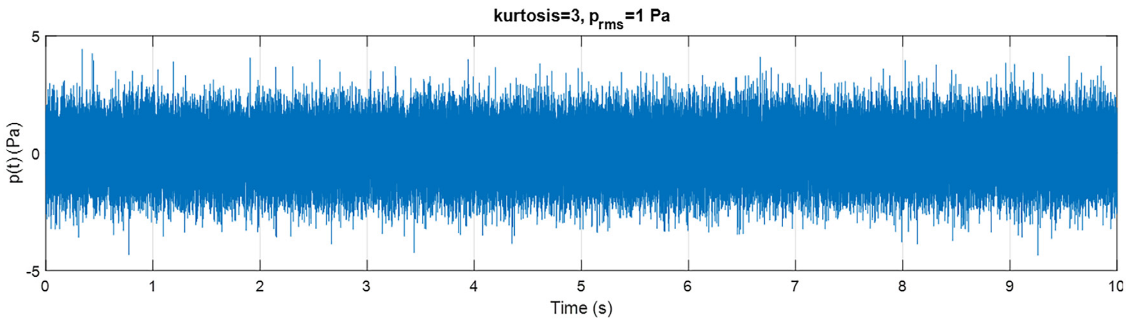

FIG. 7. (Color online) Gaussian noise with rms sound pressure of 1 Pa.

smaller amount of energy staying in the water layer. This explains the lower SEL values for silt and clay compared to sand-type sediments. The sound pressure waveform mostly includes sea surface reflections for silt and clay sediment types, while sand-type sediment results include both sea surface and sediment reflections. Therefore, the kurtosis is larger for silt and clay sediments. However, since the amplitude values are quite small, the range variation pattern becomes sensitive to very small variations after a certain range, as observed in very fine silt and clay sediment types. For the rms sound pressure results, while the variations between the different sand sediment types are small, the differences between silt and clay sediment types appear to be larger.

D. Weighted kurtosis and rms sound pressure

Time domain waveforms and kurtosis values could be different after applying auditory weighting functions because energy at some frequencies is removed (filtered out). To provide insight into the potential effect of sound on marine life, the time domain sound pressure waveforms are weighted by the auditory frequency weighting function (AFWF) based on the proposed approach by Lucke *et al.* (2024). In the following examples, the kurtosis and rms sound pressure values calculated from the weighted sound pressure waveforms are referred to as "weighted kurtosis" and "weighted rms sound pressure," respectively. In Table IV, the upper and lower frequencies for different auditory weighting functions are listed based on studies by Southall *et al.* (2019), Southall *et al.* (2007), and Lucke *et al.* (2024), respectively.

Figure 11 plots the source spectrum and auditory frequency weighting functions that were applied in this study. The AFWFs are based on studies by Southall *et al.* (2007), Southall *et al.* (2019), and Lucke *et al.* (2024). Showing the functions together on the same plot highlights the range of frequencies to which life is sensitive. Focusing on a single

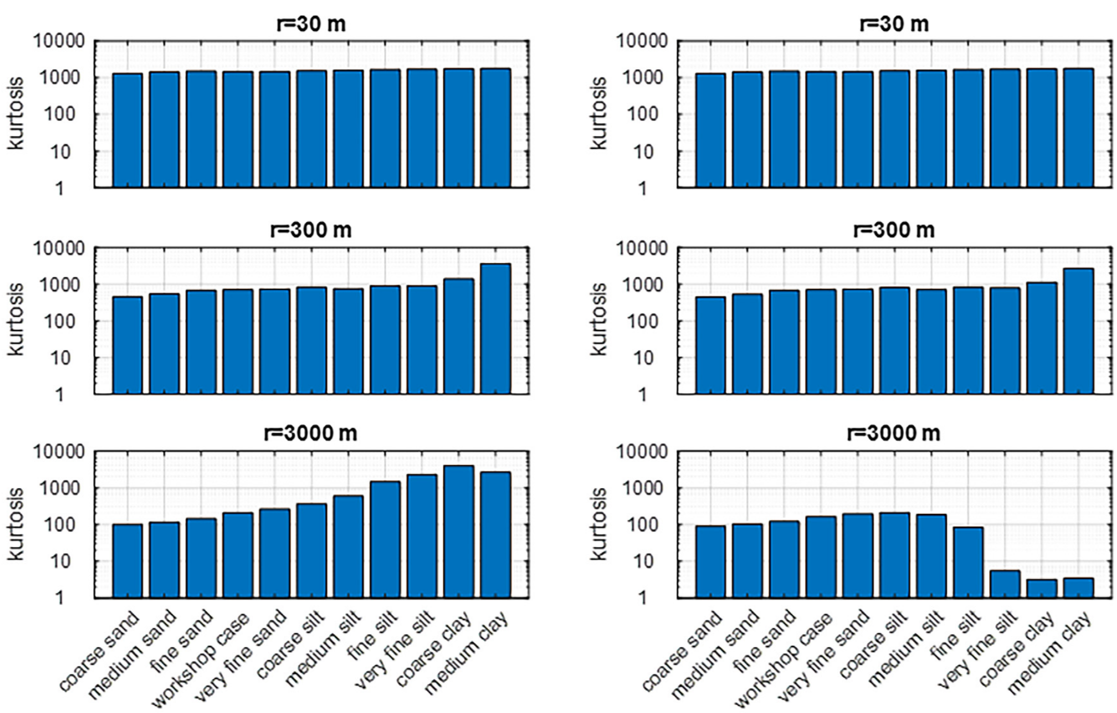

FIG. 8. (Color online) Kurtosis with (right) and without (left) additional Gaussian noise at 30, 300, and 3000 m for different sediment types. $T = 10$ s. The frequency band is between 2.818 Hz and 2818 Hz (band 1 in Table III).

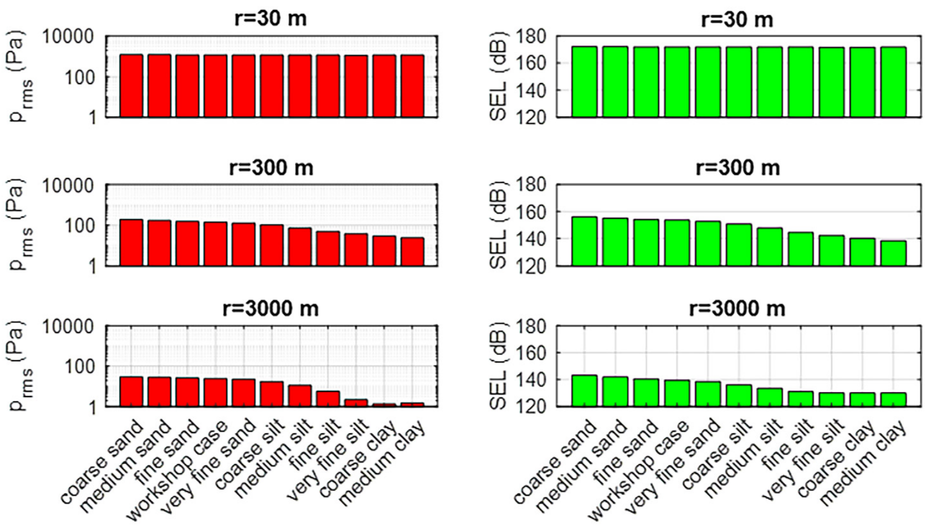

FIG. 9. (Color online) rms sound pressure (left) and SEL (right) additional Gaussian noise at 30, 300, and 3000 m for different sediment types. $T = 10$ s. The frequency band is between 2.818 Hz and 2818 Hz (band 1 in Table III).

taxon provides a skewed perspective. Notice the lack of gaps across the frequency band.

As mentioned in Sec. II, the source spectrum and transfer function were calculated for the range of 2.75 Hz to 2818.5 Hz, as defined by the JAM Workshop scenarios. Consequently, since the auditory weighting functions for high-frequency cetaceans (HF19), very high-frequency cetaceans (VHF19), and sirenians fall outside this frequency band, no examples are provided for these groups.

Selected marine mammal auditory frequency weighting functions are shown in Fig. 11. To calculate weighted kurtosis values for marine mammals, these weighting functions are applied to the time domain sound pressure with Gaussian noise.

Figure 12 shows the variation of weighted kurtosis for different sediment types. For the fishes (P1), the entire bandwidth of the transfer function of sound propagation modeling is encompassed, and therefore, results will be almost identical to the unweighted results, while for invertebrates (A1), small differences in the weighted kurtosis are visible at short range (Fig. 12).

Weighted kurtosis values exhibit a different range of variation compared to the unweighted kurtosis results shown in Fig. 10. Specifically, the weighted kurtosis for other marine carnivores in water (OCW) decreases sharply below a value of 40 beyond 400 m. These observations are based on the sediment parameters of the workshop case. When other sediment types are used, the range where kurtosis falls below 40 can be different.

The rms sound pressure is also calculated using different auditory weighting functions based on Lucke *et al.*

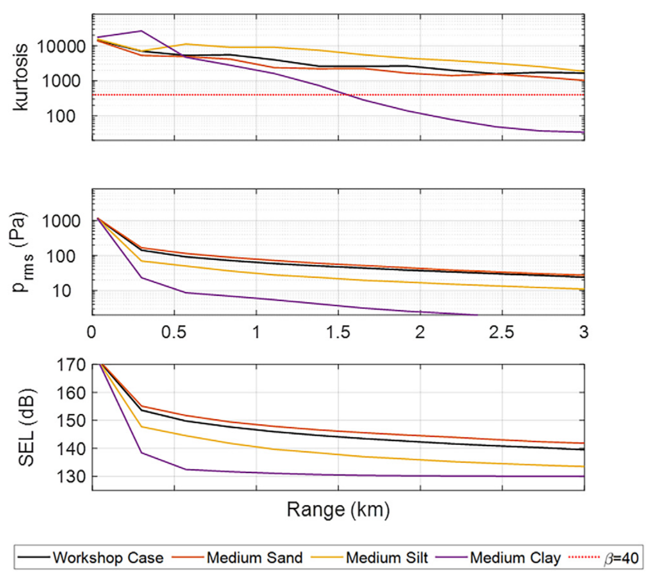

FIG. 10. (Color online) Range variation of kurtosis, rms sound pressure (Pa), and SEL re 1 $\mu Pa^2 s$ (dB) for selected sediment types. The red dotted line shows the kurtosis value of 40. $T = 10$ s. The frequency band is between 2.818 Hz and 2818 Hz (band 1 in Table III).

TABLE IV. The lower and upper roll-off frequencies, and corresponding exponents a and b, for the auditory weighting functions based on Southall *et al.* (2007) and Lucke *et al.* (2024).

	Roll-off frequency/kHz		Exponent	
Hearing group	Lower	Upper	a	b
Marine mammals (Southall *et al.*, 2019)				
Low-frequency cetaceans (LF19)	0.200	19	1	2
Other marine carnivores in water (OCW)	0.940	25	2	2
Marine mammals (Southall *et al.*, 2007)				
Low-frequency cetaceans (LF07)	0.007	22	2	2
Mid-frequency cetaceans (MF07)	0.150	160	2	2
High-frequency cetaceans (HF07)	0.200	180	2	2
Pinnipeds in water (PW07)	0.075	75	2	2
Fishes and invertebrates (Lucke *et al.*, 2024)				
Invertebrates (A1)[a]	0	0.47	N/A[c]	2
Fishes (P1)[b]	0	1.24	N/A	2

[a]A1 also applies to A3 (bony fishes without swim bladder) and A4 (bony fishes with swim bladder not involved in hearing).
[b]A2 applies to P1 (pressure sensitive, without adaptation).
[c]N/A, not applicable.

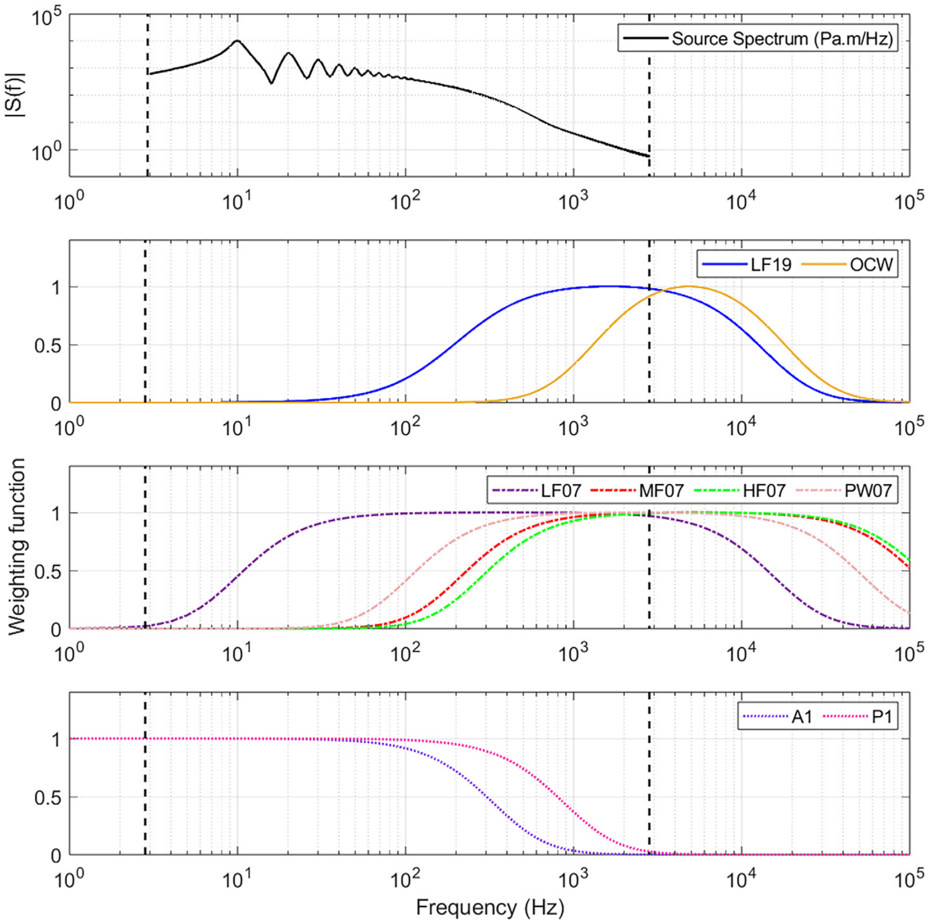

FIG. 11. (Color online) The source spectrum of single airgun (top). The lower graphs show the auditory frequency weighting functions across frequency from Southall *et al.* (2019), Southall *et al.* (2007), and Lucke *et al.* (2024).

(2024) for fish and Southall *et al.* (2007) for different marine animal groups, as shown in Fig. 13.

The dependence of rms sound pressure on the choice of frequency band and, by extension, on the auditory frequency weighting should be considered when developing impact criteria. Based on the auditory weighting function from Southall *et al.* (2007), HF cetaceans (HF07, corresponding approximately to VHF19) have the lowest rms values, followed by mid-frequency (MF) cetaceans (MF07, corresponding approximately to HF19). The rms sound pressure values used here are based on a single airgun, whereas rms sound pressure for an airgun array would be higher.

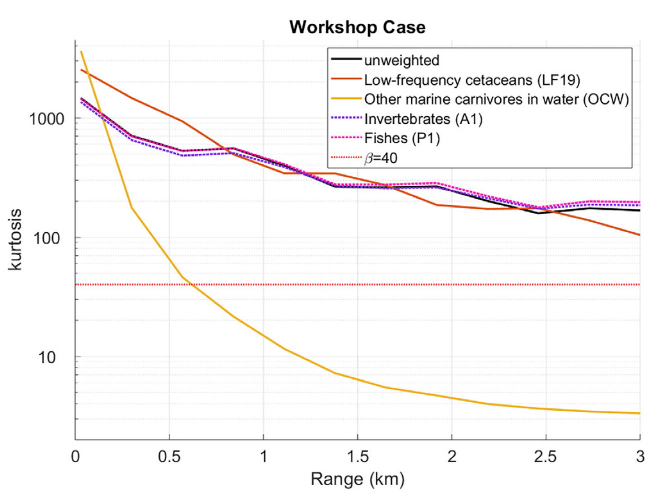

FIG. 12. (Color online) Range variation of kurtosis for the marine mammal auditory frequency weighting functions from Table IV. The red dotted line is the kurtosis value of 40. $T = 10$ s.

IV. DISCUSSION

When the threshold value of $\beta = 40$ is exceeded for the kurtosis values computed using a 1-min time window, Martin *et al.* (2020) categorize these signals as "fully impulsive." As shown in the previous examples, kurtosis depends on the environmental properties because of the influence of these on propagation. Therefore, it could be possible to see a transition from high to low kurtosis at sufficiently large distances from the source (Hastie *et al.*, 2019; Martin *et al.*, 2020). Without Gaussian noise, this transition was not clearly seen for the examples chosen in this study based on kurtosis. The effect could be seen more clearly in the measurements when the ambient sound levels are higher than the sound level of the source signal at the distant ranges. After adding Gaussian noise, a kurtosis value lower than 40 is observed for silt and clay sediments.

After adding Gaussian noise to the time domain waveform with a rms sound pressure of 1 Pa, which could be considered ambient sound (at 120 dB), lower kurtosis values were observed for silt and clay sediments. The chosen rms

https://doi.org/10.1121/10.0034709

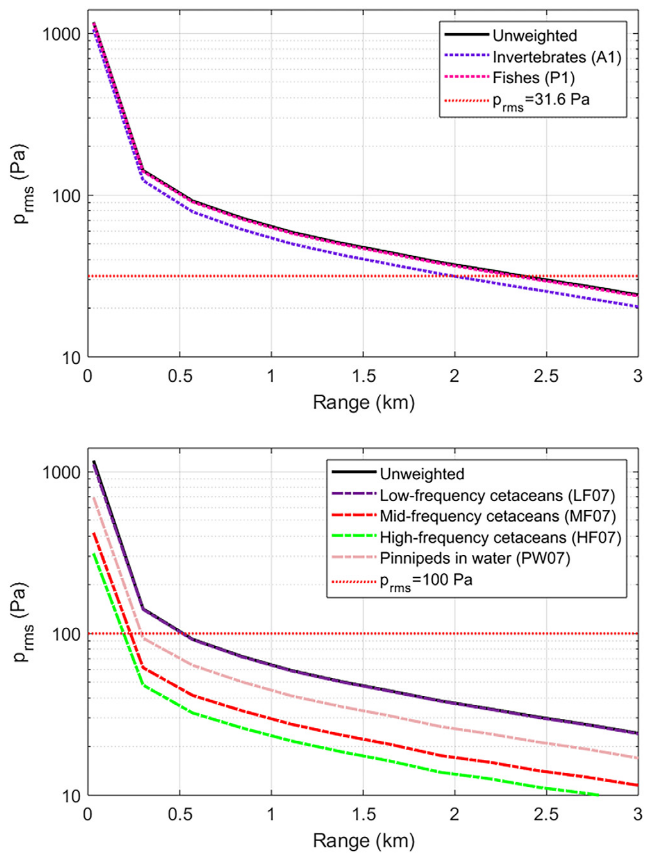

FIG. 13. (Color online) Range variation of rms sound pressure for different auditory weighting functions from Lucke *et al.* (2024) (top) for fishes and invertebrates and Southall *et al.* (2007) (bottom) for marine mammals. More details about the invertebrates and fishes are given in Table III. Sediment properties for the JAM Workshop case are used. $T = 0.1$ s. The rms sound pressure thresholds for behavioural effects are 31.6 Pa for fishes and 100 Pa for mammals (NMFS, 2023).

sound pressure for the Gaussian noise appears to be reasonable based on the NAVISON sound maps at 63 and 125 Hz for Europe (Racca *et al.*, 2024). In various locations within European waters (especially English Channel and Strait of Gibraltar), sound pressure level values can exceed 120 dB, even when averaged over a year in a single decidecade band, especially in regions with a high shipping density (Findlay *et al.*, 2023; Sertlek *et al.*, 2024). Thus, background noise can complicate measuring and interpretation of kurtosis. Whether the background noise contributes to the hearing risk depends on whether levels are substantially higher than "effective quiet levels" (Ward *et al.*, 1976), which have not been established yet for marine mammals (Finneran, 2015).

In the examples shown in this study, sediment properties are characterized only by their density, compressional wave speed, and attenuation. The observed differences in the results caused by the different sediment types considered do not include other more complicated effects that arise when the sound speed gradient or shear rigidity of the sediment is considered, i.e., sediment is described by means of layered elastic or poro-elastic models. When a more realistic description of the sediment is considered, other effects, such as soil damping, energy transferred into shear or Scholte waves, wave conversions upon wave incidence on seabed-seawater interface, and multiple soil layers, may additionally contribute to the differences in the results caused by the different sediment types. It is to be expected that the consideration of the elastic nature of a harder seabed, by means of adding its corresponding capacity to deform in shear, may alter these observations. These complicated effects are left out of discussion here.

In biological impact assessments, kurtosis-adjusted sound exposure levels for temporary threshold shift (TTS) and permanent threshold shift (PTS) are currently being investigated as an alternative metric (von Benda-Beckmann *et al.*, 2022; Zeddies *et al.*, 2023; Lucke *et al.*, 2024). Although initial results indicate that kurtosis-corrected sound exposure level may help to better predict TTS onset for intermittent signals with a wide range of kurtosis values in a small number of harbour porpoises, best model fits seem to suggest different model parameters than found for human noise studies (von Benda-Beckmann *et al.*, 2022). Various factors could be the cause of this difference, such as differences in auditory effects considered (low levels of TTS in porpoises vs PTS in humans and chinchillas), noise exposure conditions (intermittent signals vs complex impulsive continuous noise exposures), exposure duration, as well as species-specific differences in auditory system (von Benda-Beckmann *et al.*, 2022). As such, the kurtosis $\beta = 40$ condition used here to delineate between impulsive and non-impulsive should be considered indicative, and further research is required to understand whether kurtosis helps in better predicting impact of sound on marine mammal hearing for a wider range of marine mammal species under different exposure conditions. If the kurtosis adjusted metrics work well, there would be no need to distinguish between "impulsive" and "non-impulsive."

V. CONCLUSION

Acoustic propagation modelling of airgun sounds propagating in shallow waters was carried out in this study to investigate how the kurtosis and rms sound pressures are affected by different sediment properties and range. First, the propagation model SILENCE is validated through multi-model comparisons using test cases from the JAM Workshop in 2022. Good agreement is observed between SILENCE and other modeling approaches. Next, based on the time domain sound pressure results, the range variation of kurtosis and rms sound pressure is analyzed for different sediment types. For scenarios involving sand-type sediments, the sound pressure kurtosis of airgun signals decreased with increasing distance from a sound source. Conversely, in the cases of silt and clay sediment types, the duration of acoustic signals and kurtosis were less influenced by sediment reflections due to the weak reflections at the water-sediment interface. A silty/clay sediment also led to lower SELs. Similar to kurtosis, the rms sound pressure values are also affected by different sediment properties and vary by range. For the silt and clay sediment types, a faster variation in rms sound pressure is observed, which leads to lower rms sound pressures at 3000 m. As described above, this is again related to weaker reflections from the water-sediment interface and the greater sound energy transmitted to the silt and clay sediments.

Similar comparisons are conducted for the weighted kurtosis and rms sound pressure calculations for the selected invertebrates, fish, and marine mammal categories. Our modelling highlighted that due to the wide range in hearing sensitivities, kurtosis and rms sound pressure of the same signal could be very different for species groups with different hearing sensitivities. The range variations of weighted kurtosis differ from those of unweighted kurtosis. At the same time, the kurtosis and rms sound pressure also depend on the choice of bandwidth and weighting functions, as illustrated by the examples. The effects of hearing sensitivity and appropriate weighting need to be considered when developing noise impact criteria, as well as when reporting measurements of kurtosis or sound pressure.

ACKNOWLEDGMENTS

The authors thank Dr. Michael B. Porter for providing KRAKEN and SCOOTER results for the propagation loss comparisons in Fig. 3. The JAM Workshop was supported by the E&P Sound and Marine Life Joint Industry Programme.

AUTHOR DECLARATIONS

Conflict of Interest

The authors have no conflicts to disclose.

DATA AVAILABILITY

The data that support the findings of this study are available from the corresponding author upon reasonable request.

APPENDIX: MATHEMATICAL DESCRIPTION OF PROPAGATION MODEL (SILENCE)

This appendix explains the detailed derivations of SILENCE propagation model.

1. Governing equations

Cylindrical coordinates are utilized, i.e., (r, θ, z) with r representing the radial coordinate, θ representing the azimuthal coordinate and z representing the depth coordinate with the origin being positioned at the sea surface as shown in Fig. 14. The sea surface is designated as $z = z_0$, while the interface between the water and the top fluid sediment layer is positioned at z_1. Furthermore, the interfaces within the fluid sediment layer are located at $z = z_j$, where j spans from 2 to N. It is assumed that the sediment extends to infinity in the vertical direction, and a point source is positioned at a depth that is denoted as z_s.

The partial differential equations governing the dynamic response of the Pekeris waveguide in the time domain are

$$\nabla^2 p_\xi(r,z,t) - \frac{1}{c_\xi^2}\frac{\partial^2 p_\xi(r,z,t)}{\partial t^2} = 0, \tag{A1}$$

in which $\xi = w, s_j$, with w being the fluid and s_j being the sediment layer. Introducing the displacement potentials ϕ_w, ϕ_{s_j} allows one to relate the displacement to the scalar potential as follows:

$$u_\xi = \nabla\phi_\xi. \tag{A2}$$

The corresponding governing equation in the case of an inviscid acoustic fluid reads

$$\nabla^2 \phi_\xi(r,z,t) - \frac{1}{c_\xi^2}\frac{\partial^2 \phi_\xi(r,z,t)}{\partial t^2} = 0. \tag{A3}$$

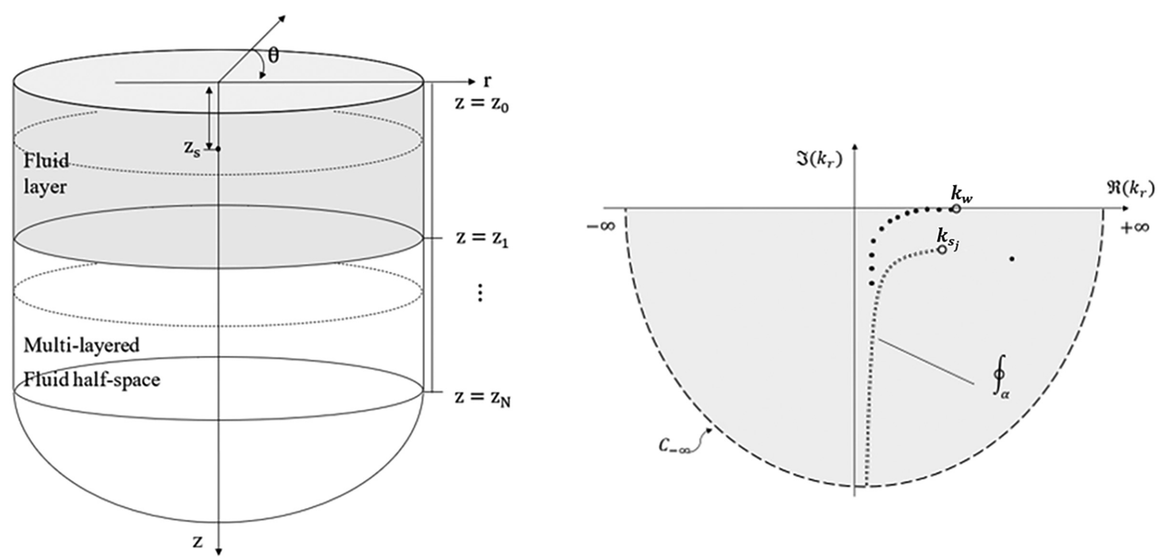

FIG. 14. Schematic depiction of the Pekeris waveguide in cylindrical coordinate (left) and visualization of complex wavenumber integration approach based on the EJP branch cut for the Pekeris waveguide (right).

In the equation above, c_ξ denotes the speeds of the compressional waves in either water or sediment. The pressure release boundary condition is imposed at the sea surface. At the water-sediment and sediment-sediment interfaces, pressure and vertical displacement continuity are imposed. The set of boundary and interface conditions reads as

$$p_w(r,\, z_0,\, t) = 0, \tag{A4}$$

$$p_w(r,\, z_1,\, t) = p_{s_1}(r,\, z_1,\, t), \tag{A5}$$

$$\begin{aligned} p_{s_j}(r,\, z_{j+1},\, t) &= p_{s_{j+1}}(r,\, z_{j+1},\, t),\\ w_{s_j}(r,\, z_{j+1},\, t) &= w_{s_{j+1}}(r,\, z_{j+1},\, t). \end{aligned} \tag{A6}$$

After performing the Fourier transformation on the boundary equation and interface equation in Eqs. (A4)–(A6) to transition into the frequency domain, the Hankel transform and complex contour integration approach are used to obtain a closed-form solution in the frequency domain as

$$\hat{f}(k_r) = \int_0^\infty f(r) J_0(k_r r) r dr, \tag{A7}$$

$$f(r) = \int_0^\infty \hat{f}(k_r) J_0(k_r r) k_r dk_r, \tag{A8}$$

in which $f(r)$ and $\hat{f}(k_r)$ denote the functions in the frequency and Hankel domains. $J_0(k_r r)$ is the Bessel function of the first kind of order zero, and k_r is the horizontal wavenumber of the medium. Transformation of the boundary equation and interface equation into the Hankel domain yields

$$\hat{p}_w(k_r,\, z_0,\, \omega) = 0, \tag{A9}$$

$$\hat{p}_w(k_r,\, z_1,\, \omega) = \hat{p}_{s_1}(k_r,\, z_1,\, \omega), \tag{A10}$$

$$\begin{aligned} \hat{p}_{s_j}(k_r,\, z_{j+1},\, \omega) &= \hat{p}_{s_{j+1}}(k_r,\, z_{j+1},\, \omega),\\ \hat{w}_{s_j}(k_r,\, z_{j+1},\, \omega) &= \hat{w}_{s_{j+1}}(k_r,\, z_{j+1},\, \omega). \end{aligned} \tag{A11}$$

2. Green's function

A pressure type (volume injection) unit amplitude point source is placed at $z = z_s$ in the water as shown in Fig. 2. The equations of motion for the displacement potential in the Hankel domain read as

$$\left[\frac{d^2}{dz^2} + k_{z,w}^2\right] \hat{\phi}_w^g(k_r, z; z_s,\, \omega) = -\frac{\delta(z - z_s)}{\rho\omega^2 2\pi}, \tag{A12}$$

$$\left[\frac{d^2}{dz^2} +_{z,s_j}^2\right] \hat{\phi}_j^g(k_r, z; z_s,\, \omega) = 0, \tag{A13}$$

in which $k_{z,\xi} = \sqrt{k_\xi^2 - k_r^2}$, with $\xi = w\, or\, s_j$ for the water or sediment layer. The solutions for the displacement potentials are the sum of a particular solution and the general solution to the homogeneous equation

$$\hat{\phi}_w^g(k_r, z; z_s,\, \omega) = \frac{1}{-\rho\omega^2} \frac{e^{-ik_{z,w}|z-z_s|}}{4\pi i k_{z,w}} + A_1^g e^{ik_{z,w} z} + A_2^g e^{-ik_{z,w} z}, \tag{A14}$$

$$\hat{\phi}_j^g(k_r, z; z_s,\, \omega) = A_{2j+1}^g e^{ik_{z,s_j} z} + A_{2j+2}^g e^{-ik_{z,s_j} z}, \tag{A15}$$

$$\hat{\phi}_N^g(k_r, z; z_s,\, \omega) = A_{2N+1}^g e^{-ik_{z,s_j} z}, \tag{A16}$$

in which the coefficients $A_i^g (i = 1, 2, \ldots, 2N+1)$ are undetermined complex amplitudes. By substituting the expressions into the boundary and interface conditions, the final set of linear algebraic equations with unknowns A_i^g is obtained. Applying the inverse Hankel transform and with the use of relationships of the Bessel functions, the Green's function in the frequency domain is obtained as

$$\tilde{\phi}_\xi^g(r, z; z_s,\, \omega) = -\frac{1}{2}\int_{-\infty}^{+\infty} \hat{\phi}_\xi^g(k_r,\, z; z_s,\, \omega) H_0^{(2)}(k_r r) k_r dk_r. \tag{A17}$$

The integral along the real axis of the complex k_r plane can be deformed by using the complex contour integration method. The expressions of the displacement potential functions in frequency are given as a summation of a finite number of poles (in the case of a fluid layer overlying a fluid half-space) supplemented by the EJP branch line integration:

$$\begin{aligned} &\tilde{\phi}_\xi^g(r, z; z_s,\, \omega)\\ &\quad = i\pi \sum_{m=1}^{M} Res\left(\hat{\phi}_\xi^g\left(k_r^{(m)},\, z; z_s,\, \omega\right) H_0^{(2)}\left(k_r^{(m)} r\right) k_r^{(m)}\right)\\ &\quad\quad -\frac{1}{2}\int_\alpha \hat{\phi}_\xi^g(k_r,\, z; z_s,\, \omega) H_0^{(2)}(k_r r) k_r dk_r. \end{aligned} \tag{A18}$$

Ainslie, M. A. (**2010**). *Principles of Sonar Performance Modeling* (Praxis Books, Springer, Berlin).
Ainslie, M. A., Halvorsen, M. B., Labak, S., Li, Z., and Lucke, K. (**2023**). JIP Acoustic Modelling (JAM) Workshop: Workshop Report, Document 02923, Version 2.1. Technical report by JASCO Applied Sciences for E&P Sound and Marine Life Joint Industry Programme [JASCO Applied Sciences (USA), Silver Spring, MD].
Ainslie, M. A., Laws, R. M., and Sertlek, H. Ö. (**2019**). "International Airgun Modeling Workshop: Validation of source signature and sound propagation models—Dublin (Ireland), July 16, 2016—problem description," IEEE J. Ocean. Eng. **44**(3), 565–574.
Ainslie, M. A., Laws, R. M., Smith, M. J., and MacGillivray, A. O. (**2024**). "Source and propagation modelling scenarios for environmental impact assessment: Model verification," J. Acoust. Soc. Am. **156**(3), 1489–1508.
Buckingham, M. J., and Giddens, E. M. (**2006**). "Theory of sound propagation from a moving source in a three-layer Pekeris waveguide," J. Acoust. Soc. Am. **120**(4), 1825–1841.
Caldwell, J., and Dragoset, W. H. (**2000**). "A brief overview of seismic airgun arrays," Leading Edge **19**(8), 898–902.
Carroll, A. G., Przeslawski, R., Duncan, A. J., Gunning, M., and Bruce, B. D. (**2017**). "A critical review of the potential impacts of marine seismic surveys on fish & invertebrates," Mar. Pollut. Bull. **114**(1), 9–24.
Collins, M. D. (**1993**). "A split-step Padé solution for the parabolic equation method," J. Acoust. Soc. Am. **93**(4), 1736–1742.
Dragoset, W. H. (**1990**). "Air-gun array specs: A tutorial," Leading Edge **9**(1), 24–32.

Erbe, C., Dent, M. L., Gannon, W. L., McCauley, R. D., Römer, H., Southall, B. L., Stansbury, A. L., Stoeger, A. S., and Thomas, J. A. (**2022**). "The effects of noise on animals," in *Exploring Animal Behavior Through Sound: Volume 1: Methods*, edited by C. Erbe and J. A. Thomas (Springer International Publishing, Cham, Switzerland), pp. 459–506.

Findlay, C. R., Rojano-Doñate, L., Tougaard, J., Johnson, M. P., and Madsen, P. T. (**2023**). "Small reductions in cargo vessel speed substantially reduce noise impacts to marine mammals," Sci. Adv. **9**(25), eadf2987.

Finneran, J. J. (**2015**). "Noise-induced hearing loss in marine mammals: A review of temporary threshold shift studies from 1996 to 2015," J. Acoust. Soc. Am. **138**(3), 1702–1726.

Gedamke, J., Gales, N., and Frydman, S. (**2011**). "Assessing risk of baleen whale hearing loss from seismic surveys: The effect of uncertainty and individual variation," J. Acoust. Soc. Am. **129**(1), 496–506.

Goley, G. S., Song, W. J., and Kim, J. H. (**2011**). "Kurtosis corrected sound pressure level as a noise metric for risk assessment of occupational noises," J. Acoust. Soc. Am. **129**(3), 1475–1481.

Guan, S., Vignola, J., Judge, J., and Turo, D. (**2015**). "Airgun inter-pulse noise field during a seismic survey in an Arctic ultra shallow marine environment," J. Acoust. Soc. Am. **138**(6), 3447–3457.

Halvorsen, M. B., Ainslie, M. A., and Dekeling, R. P. A. (**2019**). "Guest Editorial: The International Airgun Modelling Workshop," IEEE J. Ocean. Eng. **44**(3), 560–564.

Hastie, G., Merchant, N. D., Götz, T., Russell, D. J. F., Thompson, P., and Janik, V. M. (**2019**). "Effects of impulsive noise on marine mammals investigating range-dependent risk," Ecol. Appl. **29**(5), e01906.

Henderson, D., and Hamernik, R. P. (**2012**). "The use of kurtosis measurement in the assessment of potential noise trauma," in *Noise-Induced Hearing Loss: Scientific Advances*, edited by C. G. Le Prell, D. Henderson, R. R. Fay, and A. N. Popper (Springer, New York), pp. 41–55.

ISO (**2017**). ISO 18405:2017, "Underwater acoustics—Terminology" (International Organization for Standardization, Geneva), https://www.iso.org/obp/ui/en/#!iso:std:62406:en.

Kastelein, R. A., Helder-Hoek, L., Van de Voorde, S., von Benda-Beckmann, A. M., Lam, F.-P. A., Jansen, E., de Jong, C. A. F., and Ainslie, M. A. (**2017**). "Temporary hearing threshold shift in a harbor porpoise (Phocoena phocoena) after exposure to multiple airgun sounds," J. Acoust. Soc. Am. **142**(4), 2430–2442.

Küsel, E. T., and Siderius, M. (**2019**). "Comparison of propagation models for the characterization of sound pressure fields," IEEE J. Ocean. Eng. **44**(3), 598–610.

Laws, R. M., Hatton, L., and Haartsen, M. (**1990**). "Computer modelling of clustered airguns," First Break **8**(9), 331–338.

Lucke, K., MacGillivray, A. O., Halvorsen, M. B., Ainslie, M. A., Zeddies, D. G., and Sisneros, J. (**2024**). "Recommendations on bioacoustical metrics relevant for regulating exposure to anthropogenic underwater sound," J. Acoust. Soc. Am. **156**, 2508–2526.

MacGillivray, A. O. (**2006**). "An acoustic modelling study of seismic airgun noise in Queen Charlotte Basin," M.Sc. thesis, University of Victoria, Victoria, Canada, available at http://hdl.handle.net/1828/2188.

MacGillivray, A. O., and Chapman, N. R. (**2012**). "Modeling underwater sound propagation from an airgun array using the parabolic equation method," Can. Acoust. **40**(1), 19–25.

Martin, S. B., Lucke, K., and Barclay, D. R. (**2020**). "Techniques for distinguishing between impulsive and non-impulsive sound in the context of regulating sound exposure for marine mammals," J. Acoust. Soc. Am. **147**(4), 2159–2176.

Merchant, N. D., Andersson, M. H., Box, T., Le Courtois, F., Cronin, D., Holdsworth, N., Kinneging, N., Mendes, S., Merck, T., Mouat, J., Norro, A. M. J., Ollivier, B., Pinto, C., Stamp, P., and Tougaard, J. (**2020**). "Impulsive noise pollution in the Northeast Atlantic: Reported activity during 2015–2017," Mar. Pollut. Bull. **152**, 110951.

Müller, R. A. J., von Benda-Beckmann, A. M., Halvorsen, M. B., and Ainslie, M. A. (**2020**). "Application of kurtosis to underwater sound," J. Acoust. Soc. Am. **148**(2), 780–792.

NMFS (**2023**). National Marine Fisheries Service: Summary of Endangered Species Act Acoustic Thresholds (Marine Mammals, Fishes, and Sea Turtles) (National Marine Fisheries Service, Silver Spring, MD), https://www.fisheries.noaa.gov/s3/2023-02/ESA%20all%20species%20threshold%20summary_508_OPR1.pdf.

Peng, Y., Tsouvalas, A., Stampoultzoglou, T., and Metrikine, A. (**2021**). "A fast computational model for near- and far-field noise prediction due to offshore pile driving," J. Acoust. Soc. Am. **149**(3), 1772–1790.

Porter, M. B. (**1992**). The KRAKEN Normal Mode Program. Technical report jointly by Naval Research Lab and SACLANT Undersea Research Centre (Naval Research Laboratory, Washington, DC), https://apps.dtic.mil/dtic/tr/fulltext/u2/a252409.pdf.

Prior, M. K., Ainslie, M. A., Halvorsen, M. B., Hartstra, I., Laws, R. M., MacGillivray, A. O., Müller, R. A. J., Robinson, S., and Wang, L. (**2021**). "Characterization of the acoustic output of single marine-seismic airguns and clusters: The Svein Vaage dataset," J. Acoust. Soc. Am. **150**(5), 3675–3692.

Racca, R., Ainslie, M. A., Bosschers, J., Hermans, M., Lloyd, T., MacGillivray, A., Pace, F., Schuster, M., Sertlek, Ö., and Wood, M. (**2024**). "Mapping past and future shipping noise in European seas," J. Acoust. Soc. Am. **155**, A199.

Schmidt, H. (**2004**). *OASES Version 3.1 User Guide and Reference Manual* (Department of Ocean Engineering, Massachusetts Institute of Technology, Cambridge, MA), https://acoustics.mit.edu/faculty/henrik/oases.pdf.

Sertlek, H. O., and Ainslie, M. A. (**2015**). "AGORA: Airgun Source Signature Model: Its application for the Dutch Seismic Survey," in *Proceedings of Underwater Acoustics Conference and Exhibition*, Crete, Greece, pp. 439–446, available at https://www.uaconferences.org/docs/Past_proceedings/UACE2015_Proceedings.pdf.

Sertlek, H. Ö., Ainslie, M. A., and Heaney, K. D. (**2019**). "Analytical and numerical propagation loss predictions for gradually range-dependent isospeed waveguides," IEEE J. Ocean. Eng. **44**(4), 1240–1252.

Sertlek, H. Ö., and Aksoy, S. (**2013**). "Analytical time domain normal mode solution of an acoustic waveguide with perfectly reflecting walls," J. Comput. Acoust. **21**(02), 1250026.

Sertlek, H. Ö., and Blacquière, G. (**2019**). "Effects of the rough sea surface on the signature of a single air gun," IEEE J. Ocean. Eng. **44**(3), 575–581.

Sertlek, H. O., MacGillivray, A., Lloyd, T., Hermans, M., Wood, M., and Ainslie, M. (**2024**). NAVISON Final Report: Calculation and Analysis of Shipping Sound Maps for all European Seas from 2016 to 2050. Document 03436, version 1.0. Technical report by JASCO Applied Sciences (Deutschland) GmbH and Maritime Research Institute Netherlands (MARIN) for European Maritime Safety Agency (EMSA, Lisbon).

Sidorovskaia, N., and Li, K. (**2022**). "Marine compressed air source array primary acoustic field characterization from at-sea measurements," J. Acoust. Soc. Am. **151**(6), 3957–3978.

Slabbekoorn, H., Bouton, N., van Opzeeland, I., Coers, A., ten Cate, C., and Popper, A. N. (**2010**). "A noisy spring: The impact of globally rising underwater sound levels on fish," Trends Ecol. Evol. **25**(7), 419–427.

Slabbekoorn, H., Dalen, J., de Haan, D., Winter, H. V., Radford, C. A., Ainslie, M. A., Heaney, K. D., van Kooten, T., Thomas, L., and Harwood, J. (**2019**). "Population-level consequences of seismic surveys on fishes: An interdisciplinary challenge," Fish Fish. **20**(4), 653–685.

Southall, B. L., Bowles, A. E., Ellison, W. T., Finneran, J. J., Gentry, R. L., Greene, C. R., Jr., Kastak, D., Ketten, D. R., Miller, J. H., Nachtigall, P. E., Richardson, W. J., Thomas, J. A., and Tyack, P. L. (**2007**). "Marine mammal noise exposure criteria: Initial scientific recommendations," Aquat. Mamm. **33**(4), 411–521.

Southall, B. L., Finneran, J. J., Reichmuth, C. J., Nachtigall, P. E., Ketten, D. R., Bowles, A. E., Ellison, W. T., Nowacek, D. P., and Tyack, P. L. (**2019**). "Marine mammal noise exposure criteria: Updated scientific recommendations for residual hearing effects," Aquat. Mamm. **45**(2), 125–232.

Tsouvalas, A., and Metrikine, A. V. (**2014**). "A three-dimensional vibroacoustic model for the prediction of underwater noise from offshore pile driving," J. Sound Vib. **333**(8), 2283–2311.

von Benda-Beckmann, A. M., Ketten, D. R., Lam, F. P. A., de Jong, C. A. F., Müller, R. D., and Kastelein, R. A. (**2022**). "Evaluation of kurtosis-corrected sound exposure level as a metric for predicting onset of hearing threshold shifts in harbor porpoises (*Phocoena phocoena*)," J. Acoust. Soc. Am. **152**(1), 295–301.

Ward, W. D., Cushing, E. M., and Burns, E. M. (**1976**). "Effective quiet and moderate TTS: Implications for noise exposure standards," J. Acoust. Soc. Am. **59**(1), 160–165.

https://doi.org/10.1121/10.0034709

Zeddies, D. G., Denes, S. L., Lucke, K., Martin, S. B., and Ainslie, M. A. (**2023**). "Impulsive or non-impulsive: Determining hearing loss thresholds for marine mammals," in *The Effects of Noise on Aquatic Life: Principles and Practical Considerations*, edited by A. N. Popper, J. Sisneros, A. D. Hawkins, and F. Thomsen (Springer International Publishing, Cham, Switzerland), pp. 1–9.

Zhao, Y.-m., Qiu, W., Zeng, L., Chen, S.-s., Cheng, X.-r., Davis, R. I., and Hamernik, R. P. (**2010**). "Application of the kurtosis statistic to the evaluation of the risk of hearing loss in workers exposed to high-level complex noise," Ear Hear. **31**(4), 527–532.

Ziolkowski, A. M. (**1970**). "A method for calculating the output pressure waveform from an air gun," Geophys. J. Int. **21**(2), 137–161.